Semicond. Sci. Technol. **10**, 255 (1995).
2. For recent reviews discussing the connection between mesoscopic physics and quantum chaos, see B. L. Altshuler and B. D. Simons, in *Mesoscopic Quantum Physics,* E. Akkermans, G. Montambaux, J.-L. Pichard, J. Zinn-Justin, Eds. (Elsevier, Amsterdam, 1995), pp. 1–98; T. Guhr, A. Mueller-Groeling, H. A. Weidenmueller, http://xxx.lanl.gov/abs/cond-mat/9707301 (1997); Mesoscopic physics and random matrix theory are discussed in C. W. J. Beenakker, *Rev. Mod. Phys*. **69**, 731 (1997). For a general introduction to quantum chaos, see M. C. Gutzwiller, *Chaos in Classical and Quantum Mechanics* (Springer-Verlag, New York, 1990).
3. Y. M. Blanter, A. D. Mirlin, B. A. Muzykantskii, *Phys. Rev. Lett.* **78**, 2449 (1997); R. Berkovits and B. L. Altshuler, *Phys. Rev. B* **55**, 5297 (1997).
4. P. L. McEuen *et al*., *Phys. Rev. Lett.* **66**, 1926 (1991); P. L. McEuen *et al*., *Phys Rev. B* **45**, 11419 (1992).
5. R. C. Ashoori *et al*., *Surf. Sci.* **305**, 558 (1994).
6. S. Tarucha, D. G. Austing, T. Honda, R. J. van der Hage, L. P. Kouwenhoven, *Phys. Rev. Lett.* **77**, 3613 (1996).
7. A. T. Johnson *et al*., *Phys. Rev. Lett.* **69**, 1592 (1992).
8. E. B. Foxman *et al*., *Phys. Rev. B* **47**, 10020 (1993); P. L. McEuen *et al*., *Phys. B* **189**, 70 (1993).
9. J. Weis, R. J. Haug, K. von Klitzing, K. Ploog, *Phys. Rev. Lett.* **71**, 4019 (1993).
10. D. C. Ralph, C. T. Black, M. Tinkham, *ibid.* **78**, 4087 (1997).
11. K. Jauregui, W. Häusler, D. Weinmann, B. Kramer, *Phys. Rev. B* **53**, R1713 (1996); D. Weinmann, W. Häusler, B. Kramer, *Phys. Rev. Lett.* **74**, 984 (1995).
12. D. Pfannkuche and S. E. Ulloa, *Phys. Rev. Lett.* **74**, 1194 (1995).
13. O. Agam, N. S. Wingreen, B. L. Altshuler, D. C. Ralph, M. Tinkham, *ibid.* **78**, 1956 (1997).
14. L. P. Kouwenhoven *et al*., *Science* **278**, 1788 (1997).
15. C. W. J. Beenakker, *Phys. Rev. B* **44**, 1646 (1991).
16. _____ and H. van Houten, *Phys. Rev. B* **43**, 12066 (1991).
17. T. Takami, *Phys. Rev. Lett.* **68**, 3371 (1992).
18. P. Pfeffer and W. Zawadzki, *Phys. Rev. B* **52**, R14332 (1995).
19. We thank B. Altshuler, D. Ralph, and M. Heiblum for useful discussions and S. Patel and A. Huibers for valuable help throughout the measurements. We acknowledge support from Joint Services Electronics Program under grant DAAH04-94-G-0058, the Army Research Office under grant DAAH04-95-1-0331, the Office of Naval Research Young Investigator program under grant N00014-94-1-0622, and the NSF–National Young Investigator program. D.S. acknowledges the support of MINERVA grant.

19 September 1997; accepted 5 November 1997

Excitation Spectra of Circular, Few-Electron Quantum Dots

L. P. Kouwenhoven, T. H. Oosterkamp, M. W. S. Danoesastro, M. Eto, D. G. Austing, T. Honda, S. Tarucha

Studies of the ground and excited states in semiconductor quantum dots containing 1 to 12 electrons showed that the quantum numbers of the states in the excitation spectra can be identified and compared with exact calculations. A magnetic field induces transitions between the ground and excited states. These transitions were analyzed in terms of crossings between single-particle states, singlet-triplet transitions, spin polarization, and Hund's rule. These impurity-free quantum dots allow "atomic physics" experiments to be performed in magnetic field regimes not accessible for atoms.

Small solid-state devices known as quantum dots are often referred to as artificial atoms because their electronic properties resemble, for example, the ionization energy and discrete excitation spectrum of atoms (*1*). Quantum dots are usually fabricated between source and drain contacts so that the atomlike properties can be probed in current-voltage (*I-V*) measurements. Additionally, with a gate electrode nearby, the exact number of electrons N can be varied on the quantum dot by changing the gate voltage V_g. When an electron is added, the total charge on the dot changes by the elementary charge e. The associated energy change, known as the addition energy, is a combination of the single-electron charging energy and the change in single-particle energy. Charging effects and discrete single-particle states have been studied in a variety of quantum dot systems, defined not only in semiconductors but also in metal grains and molecules (*2*).

Quantum dot devices usually contain some disorder caused, for example, by impurities (*2*). Clean quantum dots, in the form of regular disks, have only recently been fabricated in a semiconductor heterostructure (*3, 4*). The circular symmetry of the two-dimensional (2D) disks gives rise to a 2D shell structure in the addition energies, analogous to the 3D shell structure in atomic ionization energies (*5*). Measurements of the ground states have shown that the 2D shells in dots are filled according to Hund's rule (*4*): Up to half-shell filling, all electrons have parallel spins; more electrons can only be added with antiparallel spins. Here we report the excitation spectra for dots with different numbers of electrons and identify the quantum numbers of the excited states. We also show the relation between spectra of successive N and how the spectra evolve with an applied magnetic field B. The relatively large dimension of quantum dots (~100 nm) allows for the use of accessible B fields that would correspond in real atoms to inaccessible fields of the order 10^6 T.

The device consists of, from bottom to top, an n-doped GaAs substrate; undoped layers of $Al_{0.22}Ga_{0.78}As$ (7.5 nm thick), $In_{0.05}Ga_{0.95}As$ (12 nm thick), and $Al_{0.22}Ga_{0.78}As$ (9.0 nm thick); and a top layer of n-doped GaAs (~500 nm thick) (Fig. 1A). A submicrometer pillar is fabricated by electron-beam lithography and etching techniques (*3*). Source and drain wires are connected to the top and substrate contacts, and a third wire is attached to the metal side gate that is placed around the pillar. The energy landscape is shown in Fig. 1B. The AlGaAs layers are insulating, but thin enough to allow for tunneling from the source to the drain through the central, disk-shaped InGaAs layer. If V_g is made more negative, the effective diameter of this disk can be reduced from a few hundred nanometers down to zero, decreasing N one by one from ~70 to zero. At a particular V_g, the excitation spectrum can be probed by increasing the source-drain voltage, V_{sd}, which opens up a transport window between the Fermi energies of the source and drain. Only ground states and excited states lying within this energy window contribute to I (see Fig. 1B). When V_g is increased, the levels in Fig. 1B shift down in energy; when an extra energy state moves through the Fermi energy of the drain, I increases. Unlike atoms, excitations do not occur inside the dot by, for instance, absorption of radiation. For dots, excitations are created when an electron tunnels out from the ground state and the next electron tunnels into an excited state. The devices are measured in a dilution refrigerator with the temperature set at 100 mK.

The differential conductance $\partial I/\partial V_{sd}$ as a function of V_{sd} and V_g is shown in Fig. 2 for N increasing from 0 to 12. Along the $V_{sd} \approx 0$ axis, N changes to $N + 1$ when adjacent diamond-shaped regions of zero current touch. The size of the diamonds is a measure of the minimum energy to add or subtract an electron. The diamonds for $N = 2$, 6, and 12 are unusually large, which correspond to filled shells (*4*). At the two upper edges of the N electron diamond, an extra electron can tunnel through the dot via the $N + 1$ electron ground state. Excited states of the N

L. P. Kouwenhoven, T. H. Oosterkamp, M. W. S. Danoesastro, Department of Applied Physics and Delft Institute of MicroElectronics and Submicrontechnology, Delft University of Technology, Post Office Box 5046, 2600 GA Delft, Netherlands.
M. Eto, Department of Physics, Faculty of Science and Technology, Keio University, 3-14-1 Hiyoshi, Kohoku-ku, Yokohama 223, Japan.
D. G. Austing, T. Honda, S. Tarucha, NTT Basic Research Laboratories, 3-1, Morinosoto Wakamiya, Atsugi-shi, Kanagawa 243-01, Japan.

+ 1 electron system that enter the transport window are seen as "lines" running parallel to the upper edges of the diamond. At the two lower edges of a diamond, an electron can tunnel out of the dot (N to $N - 1$ transitions). However, some of the lines outside the diamonds in Fig. 2 could be due to fluctuations in the density of states in the narrow leads (*6*, *7*). Below we show that lead and disk states can be distinguished by measuring $I(V_g,B)$ for different values for V_{sd} and for B being parallel to I.

The B-field dependence of the ground states is shown in Fig. 3. We have taken V_{sd} = 0.1 mV so that only ground states can lie within the transport window. The observed peaks in the current at $B = 0$ directly correspond to where the $N = 0$ to $N = 5$ diamonds touch each other in Fig. 2. The B-field dependence of the peak positions in gate voltage reflects the evolution of the ground-state energies. Besides an overall smooth B-field dependence, we observed several kinks, which we have labeled. For the regions between kinks, we can identify the quantum numbers, including the spin configurations.

Increasing V_{sd} to 3 mV yielded the data summarized in Fig. 4 (*8*). The transport window is such that I is non-zero over wider V_g ranges. Instead of the "sharp" current peaks as in Fig. 3, we now observe "stripes." Adjacent stripes sometimes overlap, implying that here eV_{sd} exceeds the addition energy. The lower edge of the Nth current stripe (which lies between the Coulomb blockade regions of $N - 1$ and N electrons) measures when the ground state of the Nth electron dot enters the transport window as V_g is made more positive. Inside a stripe, the somewhat random-looking and less pronounced changes in I are attributed to fluctuations in the density of states in the leads (*6*). However, also inside the stripes, changes in I can be seen as pronounced curves, which we argue are the excited states in the dot.

For $N = 1$, a transport window of 3 meV is too small to observe the excitations clearly. Therefore, we show in Fig. 5A the $N = 1$ stripe and a part of the $N = 2$ stripe for V_{sd} = 5 mV. For this voltage, the $N = 1$ and 2 stripes just touch at $B = 0$. A pronounced change in I [that is, from blue (<1 pA) to dark red (>10 pA)] occurs at the upper edge of the $N = 1$ stripe at $B = 0.2$ T. This change identifies the first excited state for the $N = 1$ dot [we discuss the index (0,1) below]. At higher B values, higher excited states also enter the stripe. The energy separation between the ground state and the first excited state can be read from the relative position inside the stripe. For instance, when the first excited state is two-thirds of the width of the stripe away from the ground state, the excitation energy is two-thirds of eV_{sd}. So, the excitation energy is 5 meV at $B = 0$ and decreases for increasing B. Even over this wide B range of 16 T, the first excited state never crosses with the ground state. Below 4 T, the excitation energy exceeds 3 meV; therefore, the first excited state only starts to become visible for $B > 4$ T in the first stripe of Fig. 4.

In the second, $N = 2$, stripe in Fig. 4, the first excited state crosses the ground state at $B = 4.15$ T; that is, the first excited state for $B < 4.15$ T (seen as the change in I from blue to red inside the second stripe) becomes the ground state for $B > 4.15$ T. The kink labeled by the triangle in Fig. 3 also denotes this crossing. For $N = 3$ and 4, there is also a crossing at 1.7 T in the middle of the third and fourth stripes in Fig. 4 between an up-going excited state and a down-going excited state. A similar up- and down-going crossing is seen in the ground state for $N = 5$ at 1.2 T (see also the kink in Fig. 3 labeled by the diamond).

To describe the electron states in a quantum dot, the energy spectrum $U(N,B)$ must first be calculated. In our experiment, we measured the electrochemical potential of the quantum dot, which is defined as $\mu(N) \equiv U(N) - U(N - 1)$. For a few electrons, $U(N,B)$ can be calculated exactly, including the Coulomb interactions (*9*). However, it is

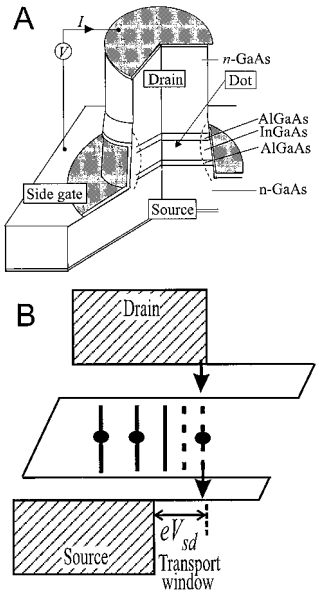

Fig. 1. (**A**) Schematic of the semiconductor layers and the metal side gate. The diameter of the pillar is 0.5 μm. (**B**) Schematic energy (horizontal axis) diagram along the vertical axis of the pillar. Hatched regions are occupied electron states in the source and drain contacts. For the case shown, two electrons are permanently trapped in the quantum dot. The third electron can choose to tunnel through the $N = 3$ ground state (solid line) or through one of the two excited states that lie in the transport window. This situation corresponds to the $N = 3$ current stripe.

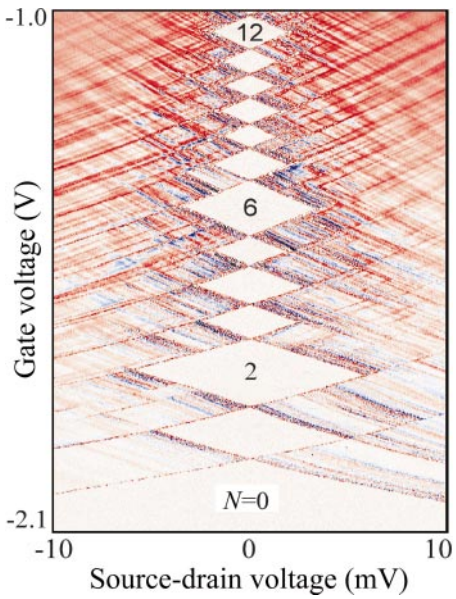

Fig. 2. Differential conductance $\partial I/\partial V_{sd}$ plotted in color scale in the $V_g - V_{sd}$ plane at $B = 0$. In the white diamond-shaped regions, $\partial I/\partial V_{sd} \approx 0$ as a result of Coulomb blockade. N is fixed in each of the diamond regions. The lines outside the diamonds, running parallel to the sides, identify excited states.

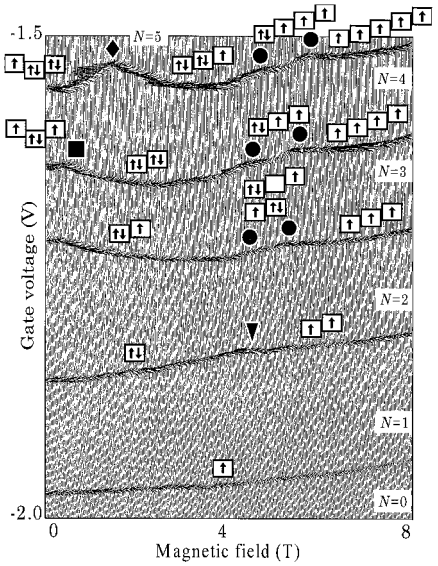

Fig. 3. Plot of $I(V_g,B)$ for $N = 0$ to 5 measured with small V_{sd} = 0.1 meV such that only ground states contributed to the current. Ground-state transitions are indicated by different symbols. The arrows in the squares indicate the spin configuration. The lowest square corresponds to a single-particle state with angular momentum $l = 0$. For squares to the right, l increases to 1, 2, 3, and so on. For $N = 4$ and 5, near $B = 0$, also the $l = -1$ square is shown on the left of the $l = 0$ square. For $N = 3$ there are two important configurations for the occupation of single-particle states in the region between the two kinks.

easier to explain the experimental results if the spectrum of noninteracting electrons in a 2D circular disk is considered first. The thickness of the thin disk freezes the electrons in the lowest state in the vertical direction. Therefore, only the confinement in the plane of the disk has to be considered, for which we take a parabolic potential $V(r) = \frac{1}{2}m^*\omega_o^2 r^2$, where $m^* = 0.06m_o$ is the effective mass of electrons in the InGaAs disk and r is the radial distance. The single-particle eigen energies with radial quantum number $n = 0, 1, 2, \ldots$ and angular momentum quantum number $l = 0, \pm 1, \pm 2, \ldots$ are given by (*10*)

$$E_{n,\ell} = (2n + |\ell| + 1)\hbar\sqrt{\left(\frac{1}{4}\omega_c^2 + \omega_o^2\right)} - \frac{1}{2}\ell\hbar\omega_c \quad (1)$$

where the cyclotron frequency $\omega_c = eB/m^*$ and $\hbar$ is Planck's constant divided by 2π. The much smaller Zeeman energy is neglected. The first few spin-degenerate states, $E_{n,\ell}$, are plotted in Fig. 6A for a confinement energy $\hbar\omega_o = 5$ meV. The two thick solid lines identify the transport window relative to the (0,0) curve for $V_{sd} = 5$ mV. The states within this stripe can be compared with the changes in I seen in the $N = 1$ stripe in Fig. 5A. The agreement is not unexpected because the noninteracting model of Eq. 1 is in fact exact for $N = 1$. We note that Eq. 1 with $\hbar\omega_o = 5$ meV fits both the ground state and the first excited state very well up to about 7 T (*11*).

If first the Coulomb interactions are neglected for $N = 2$, then the two-electron ground state energy is given by $U(N = 2) = 2E_{0,0}$, and the measured value for $\mu(2) = U(2) - U(1) = E_{0,0} = \mu(1)$. The simplest way to include interactions is to assume that the Coulomb energy E_c is independent of B. In this constant-interaction model, $\mu(2) - \mu(1) = E_c$, implying that the first and second peaks in I are separated by a constant V_g and both peaks have the same B-field dependence. The constant-interaction model has been successfully used to describe most Coulomb blockade experiments (*1*, *2*). However, as seen in Figs. 3 and 4, the $N = 1$ and 2 ground states evolve differently with B. In particular, whereas $E_{0,0}$ is the $N = 1$ ground state over the entire B range, a transition occurs at 4.15 T in the $N = 2$ ground state. To explain this transition one has to consider that the $\ell \geq 0$ orbits shrink in size when B is turned on. Two electrons in a shrinking $\ell = 0$ orbit experience an increasing Coulomb interaction. (We indeed observe in Fig. 3 that the second peak increases faster with B compared with the first peak.) The increasing Coulomb interaction will, at some B value, force one of the two electrons to occupy the larger $\ell = 1$

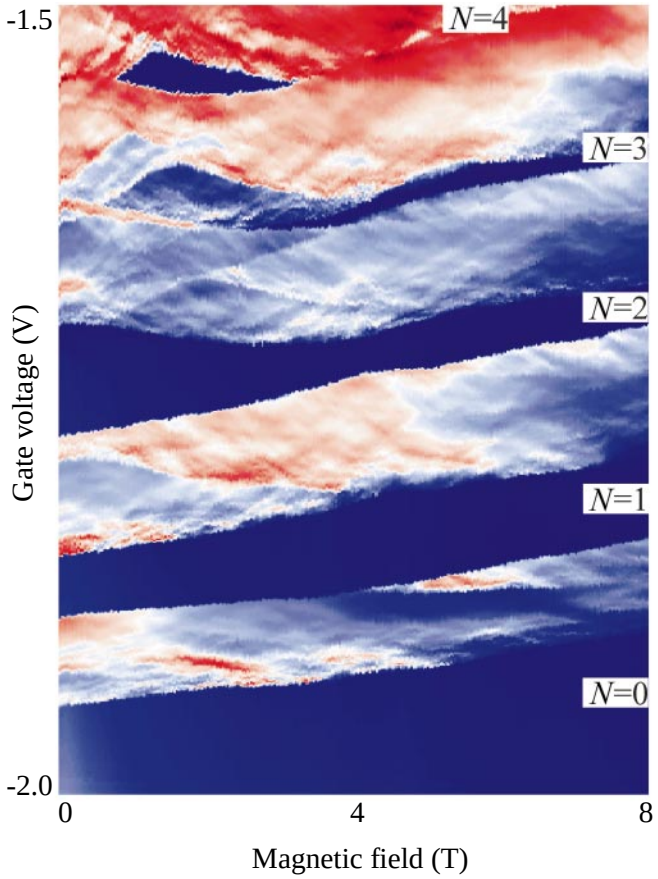

Fig. 4 (left). Plot of $I(V_g,B)$ for $N = 0$ to 4 and a part of $N = 5$ measured with $V_{sd} = 3$ meV. In the dark blue regions $I < 0.1$ pA, and in the dark red regions $I > 10$ pA. Both ground states and the first few excited states can contribute to the current. Current stripes between the Coulomb blockade regions (dark blue) for $N - 1$ and N electrons are called the N electron stripe throughout the report.

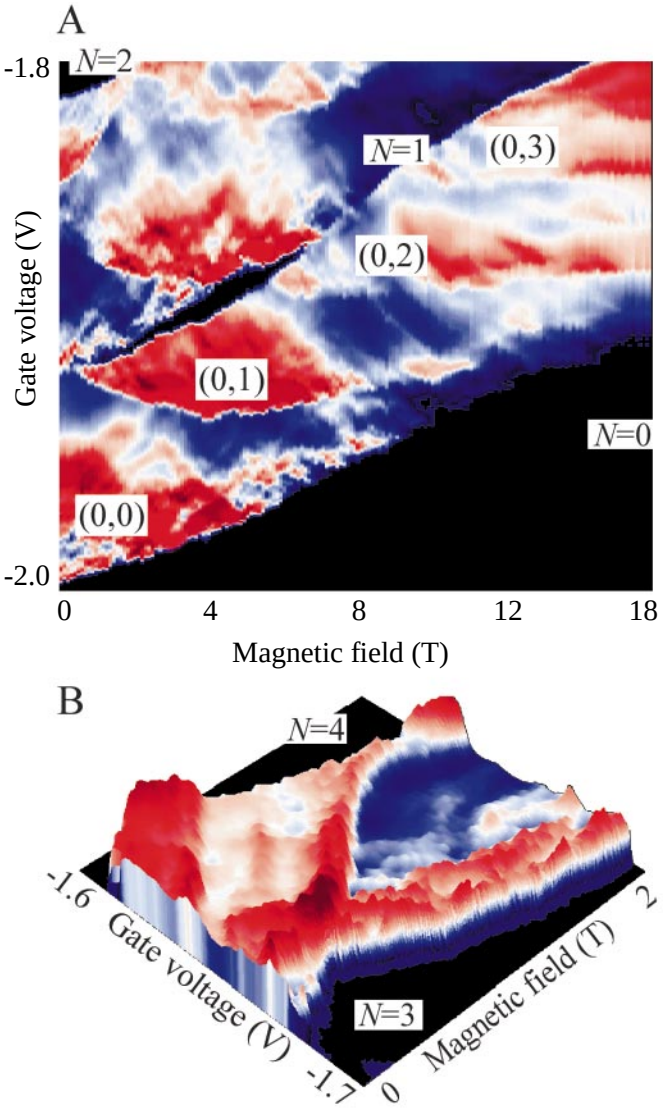

Fig. 5 (right). (**A**) Plot of $I(V_g,B)$ for $N = 1$ and 2 measured with $V_{sd} = 5$ meV up to 16 T. The states in the $N = 1$ stripe are indexed by the quantum numbers (n,l). (**B**) Surface plot of the $N = 4$ stripe measured with $V_{sd} = 1.6$ meV up to 2 T.

orbit. This transition costs kinetic energy $E_{0,1} - E_{0,0}$, but it reduces the Coulomb interaction because of the larger spatial separation between the two electrons. In addition, the system gains exchange energy when the two electrons take on parallel spins. The transition in angular momentum is thus accompanied by a transition in the total spin from the singlet $S = 0$ to the triplet state $S = 1$. An analogous singlet-triplet (S-T) transition is predicted to occur in He atoms in the vicinity of white dwarfs and pulsars at $B = 4 \times 10^5$ T (*12*). Because of the much larger size of our artificial atoms, the transition occurs at accessible fields of a few tesla. This effect was first predicted by Wagner *et al.* (*13*), and evidence for the S-T crossing has been seen (*14*).

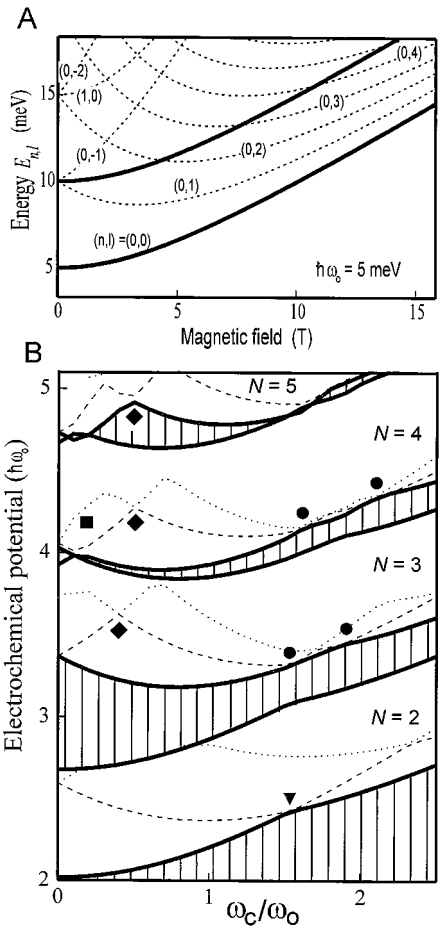

Fig. 6. (**A**) Calculated energy spectrum from Eq. 1 for $N = 1$ and $\hbar\omega_o = 5$ meV. The lowest thick line is the ground-state energy. The upper thick line is the ground-state energy shifted upward by 5 meV. Dashed states between the two thick lines can be seen in the experimental stripe for $N = 1$ in Fig. 5. (**B**) Exact calculation of energy spectra for $N = 2$ to 5. Current stripes of width 0.66 $\hbar\omega_o$ are bounded by solid lines. The Coulomb blockade regions are hatched. For $\hbar\omega_o = 5$ meV, $\omega_c = \omega_o$ corresponds to 2.8 T. The square, circle, triangle, and diamond symbols indicate the same transitions as in Fig. 3.

The exact calculation in Fig. 6B of $\mu(N)$ for the $N = 2$ to 5 ground states and first two excited states shows extra transitions between many-body states that are not included in the single-particle states of Eq. 1 (*15*). The S-T transition for $N = 2$ is one such example (*16*). In Fig. 6A, $E_{0,0}$ never crosses with $E_{0,1}$, whereas in Fig. 6B a transition, labeled by the triangle, occurs between the first (dashed) excited state and (solid) ground state at $\omega_c = 1.5\omega_o$. For $\hbar\omega_o$ 5 meV, this S-T transition is expected at $B = 4.2$ T (the experimental value is 4.15 T). The calculated second (dotted) excited state in Fig. 6B for $N = 2$ can also be seen in the second stripe of Fig. 5A (the line between blue and red current regions, which has a maximum near ~2 T).

We now discuss transitions between the first excited state and the ground state for $N = 3$, 4, and 5. The ground state for $N = 3$ has two transitions labeled by circles (Fig. 6B). On increasing B, the total spin, S, and total angular momentum, M, of the many-body states change from $(S,M) = (1/2,1)$ to $(1/2,2)$ to $(3/2,3)$. These transitions to larger angular momentum states reduce the Coulomb interactions (*1*). In addition, the spin increases in order for the electron system to gain exchange energy. A double transition in the ground-state energy is indeed observed as two kinks in the $N = 3$ trace of Fig. 3. In most regions in Fig. 3, there is one main configuration for the occupation of single-particle states. For $N = 3$, in the region between the two circle labels, there are two important configurations, which both have the same S and M. In a similar way, the $N = 4$ and 5 ground states make transitions to higher angular momentum states and an increasing total spin when B is increased. The occupation of many-body states in the region between the two circle labels is hard to determine because in this region different states lie very close in energy (see Fig. 6B). For B larger than the circle on the right, there is again a clear ground state where electrons are fully spin-polarized and they occupy successive angular momentum states.

A different type of crossing is between two excited states (crossings inside a stripe). We now argue that the crossing between two excited states in the $N = 3$ and 4 stripes labeled by diamonds in Fig. 6B is a crossing between single-particle states. For noninteracting electrons, we expect from Fig. 6A that $E_{0,0}$ and $E_{0,1}$ are the two occupied single-particle states in the ground states for both $N = 3$ and 4. The first excited state is $E_{0,-1}$ for $B < 2$ T and $E_{0,2}$ for $B > 2$ T. Together with the ground state they form a triangle. The same triangular shape is observed in both the $N = 3$ and $N = 4$ stripes in Fig. 4 where it has a maximum near 1.7 T. Continuing these arguments we expect the transition in the first excited state for $N = 3$ and 4 to become a transition in the ground state for $N = 5$. Indeed this is seen in Fig. 4 and at the kink labeled by the diamond in Fig. 3 (this transition in l from –1 to 2 is indicated in Fig. 3 in the diagrams adjacent to this kink). We emphasize that the discussion of the above crossings demonstrates a direct relation between the excitation spectrum of an N electron system with the ground state of the $N + 1$ electron system (*17*).

The last crossing we discuss is indicated by the square in Fig. 3. We identified this crossing earlier (*4*) as a manifestation of Hund's rule. As the adjacent spin diagrams show for the third and fourth electrons, a transition from parallel spins (in accordance with Hund's rule) to antiparallel spins occurs. When the states $E_{0,1}$ and $E_{0,-1}$ are sufficiently close, there is an energy gain due to the exchange interaction between electrons with parallel spins. As B is increased, $E_{0,1}$ and $E_{0,-1}$ diverge from each other (see Fig. 6A), and at some value a transition is made to antiparallel spins where the third and fourth electrons both occupy $E_{0,1}$. Figure 5B shows a surface plot of the $N = 4$ stripe measured at $V_{sd} = 1.6$ mV. This surface plot shows the B dependence of the single-particle states $E_{0,1}$ and $E_{0,-1}$, including a Hund's rule crossing between the ground state and first excited state at 0.4 T. Interestingly, a second excited state is seen with a B dependence parallel to the first excited state. Parallel first and second excited states are also seen in the calculation of Fig. 6B (see just above and below the square label in the $N = 4$ stripe). The difference between the two parallel lines is that in the lower energy line the third and fourth electrons have parallel spins (in accordance with Hund's rule) and in the higher energy line they have antiparallel spins. The energy difference is a direct measure of the exchange energy. From the experimental $N = 4$ stripe in Fig. 4 we can read directly that the gain in exchange energy is ~1 meV.

REFERENCES AND NOTES

1. R. C. Ashoori, *Nature* **379**, 413 (1996).
2. For a review, see L. P. Kouwenhoven *et al.*, *Proceedings of the Advanced Study Institute on Mesoscopic Electron Transport*, Curaçao, 25 June to 5 July 1996 (Series E, Kluwer, Dordrecht, Netherlands, in press). Also available on the World Wide Web at http://vortex.tn.tudelft.nl/mensen/leok/papers/.
3. D. G. Austing, T. Honda, S. Tarucha, *Semicond. Sci. Technol.* **11**, 212 (1996).
4. S. Tarucha, D. G. Austing, T. Honda, R. J. van der Hage, L. P. Kouwenhoven, *Phys. Rev. Lett.* **77**, 3613 (1996).
5. M. Alonso and E. J. Finn, *Quantum and Statistical Physics* (Addison-Wesley, Reading, MA, 1968).
6. T. Schmidt *et al.*, *Phys. Rev. Lett.* **78**, 1544 (1997).
7. Figure 2 actually reproduces in large detail in four different samples, implying that the structure in the density of states in the leads is not originating from a random impurity potential but probably from the lateral confinement potential of the pillar.
8. The sign of V_{sd} is such that electrons first tunnel

through the thicker barrier. In this situation, only the excited states above the ground-state electrochemical potential are observed. For equal tunnel barriers, tunneling out of the dot from excited states below the ground-state electrochemical potential can also be measured; see (*2*). Note that for a thick enough entrance barrier we can assume relaxation to the ground state between tunneling out and tunneling into the dot of the next electron.

9. See, for example, J. J. Palacios, L. Martin-Moreno, G. Chiappe, E. Louis, C. Tejedor, *Phys. Rev. B* **50**, 5760, (1994); for more references see the review by N. F. Johnson, *J. Phys. Condens. Matter* **7**, 965 (1995).
10. V. Fock, *Z. Phys*. **47**, 446 (1928); C. G. Darwin, *Proc. Cambridge Philos. Soc*. **27**, 86 (1930).
11. We believe that the smaller slopes in the experimental data of Fig. 5 for $B > \sim 7$ T are due to a changing confinement potential because screening from the leads is modified by the formation of Landau levels in the leads. This is also reflected in the changing stripe width at high B.
12. G. Thurner, H. Herold, H. Ruder, G. Schlicht, G. Wunner, *Phys. Lett*. **89A**, 133 (1982).
13. M. Wagner, U. Merkt, A. V. Chaplik, *Phys. Rev. B* **45**, 1951 (1992).
14. B. Su, V. J. Goldman, J. E. Cunningham, *ibid*. **46**, 7644 (1992); R. C. Ashoori *et al*., *Phys. Rev. Lett*. **71**, 613 (1993); T. Schmidt *et al*., *Phys. Rev. B* **51**, 5570 (1995).
15. For details of the calculation see M. Eto, *Jpn. J. Appl. Phys*. **36**, 3924 (1997). In the numerically exact calculations, every electron is assumed to occupy one of the lowest 15 single-particle states at $B = 0$. The strength of the Coulomb interaction is fixed such that $e^2/\varepsilon\sqrt{\hbar/m^*\omega_o} = \hbar\omega_o$ (ε is the permittivity). (Interactions between electrons in the dot and in the leads are neglected.) The calculated results indicate that the many-body states consist of one main configuration [two main configurations for $N = 3$ and $(S,M) = (½,2)$] and several small contributions from other configurations. The depicted configurations in Fig. 3 overlap by ~70% or more with the many-body ground states (the spin-polarized states overlap by more than 95%).
16. For a theoretical analyses of the $N = 2$ excitation spectrum, see, for example, D. Pfannkuche, R. R. Gerhardts, P. A. Maksym, V. Gudmundsson, *Physica B* **189**, 6 (1993).
17. Also for $N \sim 100$ quantum dots the excitation spectra of N and $N + 1$ can be strongly correlated, as observed recently by D. R. Stewart *et al*. [D. R. Stewart, D. Sprinzak, C. M. Marcus, C. I. Duruöz, J. S. Harris Jr., *Science* **278**, 1784 (1997)].
18. We thank R. J. van der Hage, J. Janssen, Y. Kervennic, J. E. Mooij, S. K. Nair, L. L. Sohn, Y. Tokura, and T. Uesugi for help and discussions. Supported by the Dutch Foundation for Fundamental Research on Matter. L.P.K. was supported by the Royal Netherlands Academy of Arts and Sciences.

21 July 1997; accepted 8 October 1997

Coupled Quantum Dots Fabricated by Cleaved Edge Overgrowth: From Artificial Atoms to Molecules

Gert Schedelbeck, Werner Wegscheider,* Max Bichler, Gerhard Abstreiter

Atomically precise quantum dots of mesoscopic size have been fabricated in the gallium arsenide–aluminum gallium arsenide material system by cleaved edge overgrowth, with a high degree of control over shape, composition, and position. The formation of bonding and antibonding states between two such "artificial atoms" was studied as a function of quantum dot separation by microscopic photoluminescence (PL) spectroscopy. The coupling strength within these "artificial molecules" is characterized by a systematic dependence of the separation of the bonding and antibonding levels, and of the PL linewidth, on the "interatomic" distance. This model system opens new insights into the physics of coupled quantum objects.

Over the last 5 years, quantum dots (QDs)—boxes in which charge carriers are quantum-confined in three dimensions—have been realized in semiconductors (*1*–*11*). Although these QDs are commonly part of a single crystalline solid, their properties are in many ways analogous to those of atoms (*10*); a "shell-like" energy staircase for single-electron charging (*11*) and extremely narrow homogeneous linewidths in optical spectra have been observed (*6*). The growing interest in QD systems is not only of a fundamental nature but is strongly driven by applications such as semiconductor laser devices, where discrete energy level schemes should be advantageous in many respects (*12*).

A diverse range of technologies, including high-resolution electron beam lithography and focused laser beam writing, have been implemented to fabricate such "artificial atoms" from layers prepared by molecular beam epitaxy (MBE); such layers often serve as starting material because quantum confinement along the growth direction can be readily achieved (*1*, *2*). Unfortunately, QDs confining excitons of high optical quality whose emission is governed by narrow "atom-like" lines must be prepared differently. In the GaAs-AlGaAs material system, their size must be in the 10-nm range, the equivalent of the hydrogen-like Bohr orbit for excitons. The latter represent quantized excitations in a semiconductor in the form of electrostatically bound electron hole pairs.

To date, the realization of such QDs has relied on monolayer thickness fluctuations of thin quantum wells (QWs) (*3*–*6*) or on spontaneous island formation during strained layer epitaxy (*7*–*9*). These structures have the advantage that they contain few crystal imperfections, which are inevitably accompanied by a high number of nonradiative recombination centers. However, as a consequence of the inherent randomness in the formation process of ensembles of such natural and self-organized QDs, they differ in size and shape, and their position is not under precise experimental control. Therefore, highly local spectroscopic techniques are essential to extract the properties of individual objects. The long-standing question of whether the analogy between QDs and artificial atoms can be taken even further—that is, whether coupled QDs act like coupled atoms in a molecule (*13*)—must therefore be answered in a different kind of experiment.

Here, we report on the fabrication of individual and coupled QDs of high optical quality whose size, shape, and position are completely engineered by the fabrication process. Starting from an artificial atom characterized by a homogeneous linewidth as narrow as 70 μeV (full width at half maximum, FWHM) in optical emission spectra, the formation of an "artificial molecule" can be observed as the coupling strength is gradually increased. As coupling between two QDs is introduced, the sharp resonance resulting from ground-state exciton transitions of an isolated dot splits into a pair of lines. The splitting as well as the peak widths systematically increase with increasing coupling strength.

This scenario of an exciton bound to two quantum-mechanically coupled QDs can be compared to the synthesis of a positively charged hydrogen molecule H_2^+ from an electron and two protons; such a system can be described in the framework of elementary quantum mechanics by the formation of bonding and antibonding states. In contrast to previous work on coupled Coulomb islands, which were explained in terms of classical interdot capacitance coupling (*2*), the excitonic states in our QDs are quantum-mechanically coupled and can be thought of as a coherent wave that is delocalized over the two dots. Such widely adjustable, coherently coupled QDs seem to be ideally suited for fundamental studies in a regime that is inaccessible to experiments on real atoms.

Our sample design is based on quantum

Walter Schottky Institut, Technische Universität München, Am Coulombwall, D-85748 Garching, Germany.

*To whom correspondence should be addressed. E-mail: wegscheider@wsi.tu-muenchen.de